ChemComm

COMMUNICATION

View Article Online
View Journal | View Issue

Cite this: *Chem. Commun.*, 2015, **51**, 15125

Received 13th July 2015,
Accepted 19th August 2015

DOI: 10.1039/c5cc05788d

www.rsc.org/chemcomm

Ultrathin $HNbWO_6$ nanosheets: facile synthesis and enhanced hydrogen evolution performance from photocatalytic water splitting†

Yuhao Liu, Jinhua Xiong, Shuiguang Luo, Ruowen Liang, Na Qin, Shijing Liang* and Ling Wu*

Ultrathin monolayer $HNbWO_6$ nanosheets have been successfully prepared through a simple and ultrafast ion intercalation assisted exfoliation method. These obtained highly dispersed nanosheets present enhanced photocatalytic hydrogen evolution activity compared to the nanosheets prepared by the traditionally time-consuming process.

The discovery of the physical exfoliation of graphite into merely one carbon atom thick graphene single sheets has triggered the exponential growth of research and development of this fascinating ultrathin nanomaterial.[1] These single sheets, so-called nanosheets, can be regarded as a new class of materials, which have an extremely small thickness of ~1 nm and are up to several tens of micrometers in lateral size.[2,3] In particular, ultrathin metal oxide nanosheets have drawn tremendous attention owing to their various elemental composition and distinctive properties, such as high surface area, anisotropic features, and single-crystalline texture.[4–6] The unique characteristics of these nanostructures make them functional materials in fields including cosmetics,[7] optoelectronics[8] and heterogeneous photocatalysis.[9–12] More importantly, the single molecular layers of these materials provide an opportunity for the understanding of the photocatalytic reaction at the molecular level.[13,14]

Generally, the effective methods of approach to the synthesis of two-dimensional (2D) nanosheets can be divided into two major categories: "top-down" and "bottom-up" methods according to the process of creating nanoscale structures.[15–18] Until now, several ultrathin metal oxide nanostructures have been prepared using a bottom-up approach through either the vapor deposition method[19] or wet-chemical one-pot synthesis,[20,21] but this approach needs the molecular or atomic components to build more complex nanoscale assemblies or directed self-assemblies based on complex mechanisms and technologies.[22,23] Therefore, ultrathin nanosheets are mainly prepared using a much milder top–down approach through ion-exchange, intercalation, swelling, mechanical shaking and subsequent reassembly processes.[24,25] However, this type of exfoliation is considered to be time-consuming owing to slow diffusion processes and takes typically 1–2 weeks according to several reports.[26] In view of this, it is necessary to develop a very rapid and time-efficient approach for the preparation of 2D metal oxide nanosheets.

Herein, we report an efficient, simple method towards the ultrafast synthesis of ultrathin metal oxide nanosheets based on an acid–base reaction and ion intercalation assisted exfoliation strategy. Simply by dispersing the layered parent of $HNbWO_6 \cdot 1.5H_2O$ in the polar amine of triethanolamine aqueous solution, translucent colloidal nanosheet suspensions can be obtained in just a few minutes. Scheme 1 illustrates the procedure for the fabrication of 2D ultrathin $HNbWO_6$ nanosheets. It is found that thus obtained well-dispersed ultrathin monolayer $HNbWO_6$ nanosheet suspensions exhibit an efficient photocatalytic H_2 evolution performance *via* an *in situ* reaction under simulated sunlight irradiation. Moreover, highly dispersed and hyperfine Pt nanoparticle loading on the ultrathin $HNbWO_6$ nanosheets *via* an *in situ* photodeposition method showed a remarkable promotion for photocatalytic hydrogen production.

Monolayer $HNbWO_6$ nanosheet suspensions were synthesized rapidly using triethanolamine (TEOA) (see the ESI† for details).

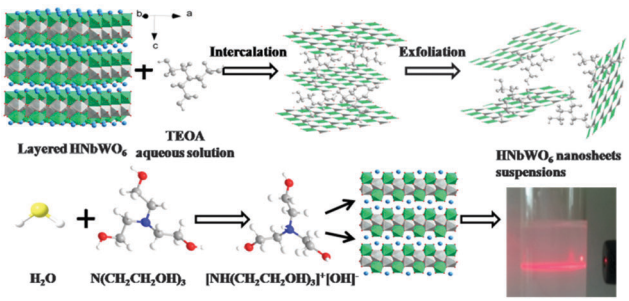

Scheme 1 Scheme illustrating the preparation of ultrathin $HNbWO_6$ nanosheets through the acid–base reaction and ion intercalation assisted exfoliation strategy.

State Key Laboratory of Photocatalysis on Energy and Environment, Fuzhou University, Fuzhou 350002, P. R. China. E-mail: wuling@fzu.edu.cn, sjliang2011@gmail.com; Fax: +86-591-83779105, +86-591-22866070; Tel: +86-591-83779362, +86-591-18060611675

† Electronic supplementary information (ESI) available. See DOI: 10.1039/c5cc05788d

The samples are denoted as N-$HNbWO_6$. Restacked $HNbWO_6$ nanosheet aggregates synthesized using the traditional approach with tetra-*n*-butylammonium hydroxide (TBAOH) are denoted as T-$HNbWO_6$. Structural analysis of the synthetic samples was carried out by XRD (Fig. S1, ESI†). The single-phase diffraction pattern of layered $LiNbWO_6$ and $HNbWO_6$ samples matches well with the published data (JCPDS: 41-0378 and 41-0110, respectively). The characteristic (002) peak shifted to a lower 2θ angle after the proton-exchange process, indicating that the interlayer distance of $HNbWO_6$ (d = 1.30 nm) is wider than that of $LiNbWO_6$ (d = 0.93 nm). This will be beneficial for the intercalation of an organic base in a subsequent exfoliation process. Compared with the layered parent compounds, $HNbWO_6$ nanosheets obtained using this rapid acid–base reaction method with TEOA aqueous solution lost their periodic layered structure and long-range order characteristics in c axial direction, only showing a few weak in-plane diffraction peaks of (110), (200) and (220).[15] Owing to the disordered restacking, the (002) peak further shifted to a lower 2θ angle at 6.34°. These results are consistent with the T-$HNbWO_6$ nanosheets.

A typical layer structure of $LiNbWO_6$ and $HNbWO_6$ was observed to be stacked layer by layer from the SEM images shown in Fig. S2a (ESI†) and Fig. 2b, respectively. These layered metal oxides consist of tabular particles with a size of 3–20 μm, while the thickness of layered $HNbWO_6$ flakes is about 50 nm. The image of the $HNbWO_6$ nanosheets prepared by this rapid acid–base reaction method indicates the formation of a random aggregation of rather loose and irregular 2D nanosheets (Fig. S2c, ESI†).[27] This image is similar to that of the nanosheets obtained using the traditional method (Fig. S2d, ESI†). The morphology of these rapidly synthesized nanosheets was further confirmed by TEM and HRTEM images (Fig. 1). The individual sheets are obtained using this approach (Fig. 1a), with edge lengths of several hundred nanometers. Note that at the edge of the nanosheets, nanotubes were formed by the rolling up of exfoliated $HNbWO_6$ nanosheets. The produced nanotubes were usually 40–50 nm in diameter and several hundred nanometers in length.[28] The difference of chemical exfoliation reagents caused the cooperative distortion of MO_6 octahedra in $HNbWO_6$, which might become a source of internal stress and induce the rolling-up behavior.[29,30] The $HNbWO_6$ nanosheet suspensions obtained using this method has an obvious Tyndall effect shown in Fig. 1a, inset, indicating the formation of freestanding and homogeneous 2D ultrathin nanosheets. As shown in Fig. 1b, the SAED analysis of an individual nanosheet reveals some bright spots with the single crystalline feature, which can be indexed as the [001] zone axis of the tetragonal lattice in planar orientation. The HRTEM image (Fig. 1c) shows a clear lattice structure, which demonstrates that the $HNbWO_6$ nanosheets retain a high in-plane crystallinity. The angle labeled in the enlarged HRTEM image (Fig. 1d) is 90°, which is in agreement with the theoretical value of the angle between the (010) and (100) planes. The clear fringes have a lattice spacing of 0.33 nm, which corresponds to the (110) plane of tetragonal $HNbWO_6$. Visualization of the nanosheets can be realized by atomic force microscopy (AFM) shown in Fig. 1e, exfoliated nanosheets with a lateral size in the range of submicrometers, and most of the measured

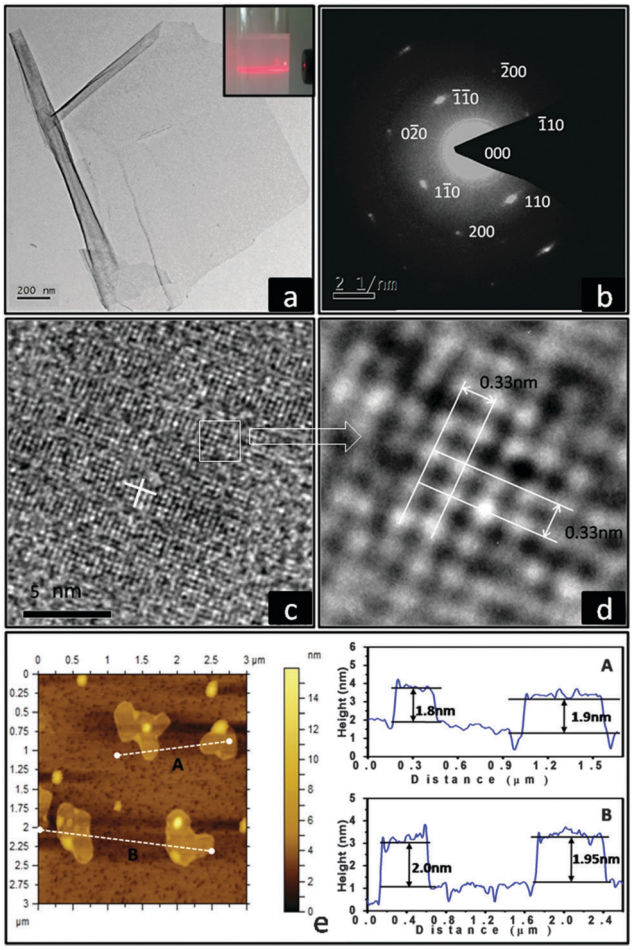

Fig. 1 (a) TEM images of ultrathin $HNbWO_6$ nanosheet suspensions. The inset in (a) is the photograph of the colloidal $HNbWO_6$ nanosheet dispersions. The light beam is incident from the side to demonstrate the Tyndall effect. (b) SAED and (c) HRTEM images taken from a part of a single nanosheet. (d) HRTEM image enlarged from (c). (e) Representative AFM image (left) and corresponding thickness analysis (right) taken around the white line in left.

thickness values of single layer $HNbWO_6$ nanosheets are between 1.8 and 2.0 nm. This result well matched the expected value of the thickness of the $HNbWO_6$ layer (Fig. S3, ESI†), indicating that the as-prepared $HNbWO_6$ nanosheets were monolayered. The difference between experimental height and slab thickness might arise from the distortion of the monolayer nanosheet and the adsorption of triethanolamine molecules and water molecules on the surface of the nanosheets (see Fig. S4, ESI†). Such a behavior was in accordance with previous results for oxide nanosheet systems.[31,32]

In addition, energy dispersive X-ray spectrometry (EDS) analysis was conducted to confirm the composition of these $HNbWO_6$ nanosheets (Fig. S5a, ESI†). The elements, Nb, W and O, were all detected. The EDS mapping in Fig. S5b (ESI†) clearly shows the strong signals for Nb, W and O, further confirming that this method is an effective and fast method for preparing ultrathin nanosheets. In conclusion, the above mentioned results provide direct and solid evidence of the formation of monolayer $HNbWO_6$ nanosheets. For comparison, the TEM and

AFM of $HNbWO_6$ nanosheets prepared by the traditional method with TBAOH aqueous solution are also shown in Fig. S6a and b (ESI†), respectively. All these results indicate that this method is more advantageous than the traditional approach for the preparation of monolayer $HNbWO_6$ nanosheets. The introduction of TEOA as a stripping agent based on an acid–base reaction and ion intercalation process is a key factor that promotes the exfoliation of the layered precursors. It is believed that the amine end of the TEOA tends to accept a proton from water because of the presence of lone electron pairs, generating $[HN(CH_2CH_2OH)_3]^+[OH]^-$, which can passively diffuse between the two regions along with H^+ and OH^-. *In situ* information of $[HN(CH_2CH_2OH)_3]^+[OH]^-$ between the neighboring layers offered this layered material for stripping.[33–35] We also demonstrated that this method was suitable to obtain $HNbxTa1\text{-}xWO_6$ (x = 0.7, 0.5, 0.3, 0) ultrathin nanosheets (see Fig. S7, ESI†), suggesting the generality of the protocol. In addition, the stripping agent can also be replaced with other polar amines of triisopropanolamine (TIPA) for the efficient and ultrafast preparation of ultrathin $HNbWO_6$ nanosheets (see Fig. S8, ESI†).

The BET surface area of restacked $HNbWO_6$ nanosheets prepared using TEOA and TBAOH aqueous solutions is about 41.4 and 84.5 $m^2\ g^{-1}$, respectively, which is larger than that of layered $HNbWO_6$ nanosheets (10.7 $m^2\ g^{-1}$). The adsorption–desorption isotherm of restacked $HNbWO_6$ nanosheets is a type IV isotherm, whereas the layered $HNbWO_6$ displays the type II isotherm (Fig. S9a, ESI†). The pore size distribution of restacked nanosheets mainly ranges from 0.1 to 30 nm (Fig. S9b, ESI†), suggesting that the as-exfoliated $HNbWO_6$ maintains the free-standing nanosheet form. The band gap energy and electronic properties of prepared nanosheets were calculated from UV-vis diffuse reflectance spectra and Mott–Schottky measurements, respectively. As shown in Fig. S10 (ESI†), the flat-band potential of N-$HNbWO_6$, T-$HNbWO_6$ and L-$HNbWO_6$ was *ca.* −0.88 V, −0.84 V and −0.94 V *vs.* Ag/AgCl at pH 6.8, respectively, corresponding to *ca.* −0.68 V, −0.64 V and −0.74 V *vs.* NHE at pH 6.8, respectively, which is more negative than the H_2O/H_2 potential (−0.41 V *vs.* NHE at pH 6.8). Therefore, it is thermodynamically permissible for the transformation of photogenerated electrons into H_2O to produce H_2.

Using these highly dispersed monolayer $HNbWO_6$ nanosheet suspensions as heterogeneous photocatalysts, H_2 evolution reactions were conducted under simulated sunlight irradiation (Fig. S11, ESI†). For comparison, the photocatalytic performances of restacked $HNbWO_6$ nanosheets obtained with TBAOH were further evaluated by redispersing them in the TEOA aqueous solution. As presented in Fig. 2, N-$HNbWO_6$ and T-$HNbWO_6$ show negligible activity for hydrogen evolution without Pt modification. In contrast, the activity of both improved remarkably with the Pt loading due to the Schottky barrier junctions. Moreover, the average hydrogen production rate of N-$HNbWO_6$ is strikingly higher than T-$HNbWO_6$. The reduction in the activity of T-$HNbWO_6$ could be attributed to a mild blockage of surface sites by the adsorption of bulkier TBA^+ cations.[26] The TEM of restacked $HNbWO_6$ nanosheets (Fig. S12, ESI†) also further confirmed that these aggregates were comprised of irregularly

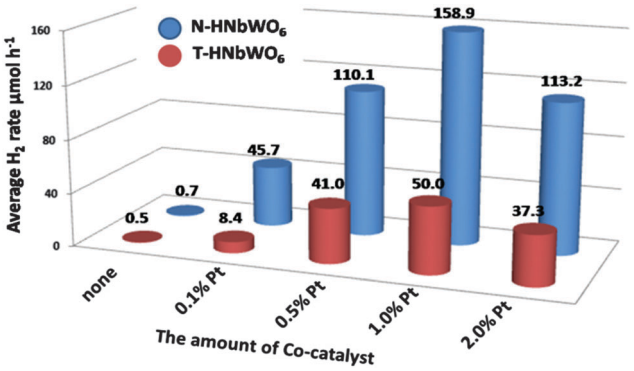

Fig. 2 Average H_2 evolution rate of N-$HNbWO_6$ and T-$HNbWO_6$ loaded with different amounts of the Pt co-catalyst reaction for five hours.

stacked and folded nanosheets, and no single sheets were observed. Furthermore, the hydrogen production amount of 1.0 wt% Pt loaded N-$HNbWO_6$ reached up to 794.5 μmol for five hours (with a stable H_2 evolution rate of 158.9 μmol h^{-1}), which was much higher than that of T-$HNbWO_6$ (Fig. S13, ESI†). The apparent quantum yield of 1.0 wt% Pt loaded N-$HNbWO_6$ and T-$HNbWO_6$ was 14.1% and 2.4%, respectively (Fig. S14, ESI†).

In heterogeneous photocatalysis, the size and uniformity of a co-catalyst have a significant impact on the photocatalytic water splitting performance, and the smaller size and high dispersion of cocatalyst particles are more active for H_2 evolution.[36,37] From Fig. 3a and b, the Pt nanoparticles anchored on these nanosheet suspensions were smaller and more dispersed, while some Pt particle agglomerates were formed on the restacked T-$HNbWO_6$ nanosheets. Thus, the enhancement of the photocatalytic activity of the well-dispersed ultrathin monolayer nanosheet suspensions can be attributed to much higher dispersion and smaller size of Pt nanoparticles anchored onto their surfaces. ICP results show that the percentage of Pt in the samples N-$HNbWO_6$ and T-$HNbWO_6$ was 0.88% and 0.92%, respectively, further revealing that the difference in the activities between these two samples was not caused by the different contents of Pt loading. All these results indicate that highly dispersed and hyperfine Pt nanoparticles were key factors for the enhanced photocatalytic H_2 production activity of N-$HNbWO_6$.

In summary, ultrathin $HNbWO_6$ nanosheets have been successfully obtained *via* an ultrafast, simple and efficient

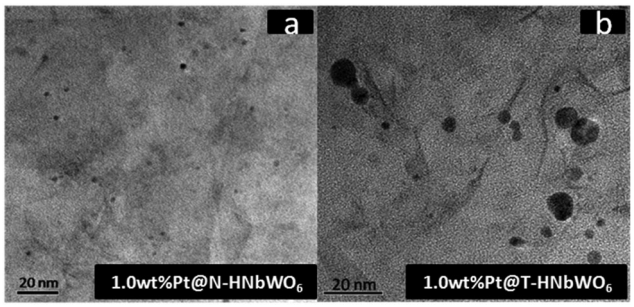

Fig. 3 TEM images of 1.0 wt% Pt loaded N-$HNbWO_6$ (a) and T-$HNbWO_6$ nanosheets (b).

exfoliation method based on an acid–base reaction and ion intercalation strategy. The as-prepared $HNbWO_6$ ultrathin nanosheet suspensions are stable and highly dispersed. Compared with the $HNbWO_6$ nanosheet aggregates prepared using TBAOH aqueous solution, the ultrathin $HNbWO_6$ nanosheet suspensions showed efficient activity for photocatalytic H_2 evolution, due to the *in situ* deposition of smaller and highly dispersed noble-metal clusters. We believe that our strategy could be broadly applied for the facile production of other ultrathin nanostructures with great potential for use in various applications.

This work was supported by the National Natural Science Foundation of China (21177024, 21303019 and 21273036) and the Natural Science Foundation of Fujian Province (2014J05016).

Notes and references

1 K. S. Novoselov, A. K. Geim, S. Morozov, D. Jiang, Y. Zhang, S. A. Dubonos, I. Grigorieva and A. Firsov, *Science*, 2004, **306**, 666–669.
2 T. Shibata, G. Takanashi, T. Nakamura, K. Fukuda, Y. Ebina and T. Sasaki, *Energy Environ. Sci.*, 2011, **4**, 535–542.
3 L. Wang and T. Sasaki, *Chem. Rev.*, 2014, **114**, 9455–9486.
4 S. I. Shin, A. Go, I. Y. Kim, J. M. Lee, Y. Lee and S.-J. Hwang, *Energy Environ. Sci.*, 2013, **6**, 608–617.
5 M. Xu, T. Liang, M. Shi and H. Chen, *Chem. Rev.*, 2013, **113**, 3766–3798.
6 S. Z. Butler, S. M. Hollen, L. Cao, Y. Cui, J. A. Gupta, H. R. Gutierrez, T. F. Heinz, S. S. Hong, J. Huang and A. F. Ismach, *ACS Nano*, 2013, **7**, 2898–2926.
7 A. López-Galindo, C. Viseras and P. Cerezo, *Appl. Clay Sci.*, 2007, **36**, 51–63.
8 M. Osada and T. Sasaki, *Adv. Mater.*, 2012, **24**, 210–228.
9 T. W. Kim, S. G. Hur, S.-J. Hwang, H. Park, W. Choi and J.-H. Choy, *Adv. Funct. Mater.*, 2007, **17**, 307.
10 J. L. Gunjakar, T. W. Kim, H. N. Kim, I. Y. Kim and S.-J. Hwang, *J. Am. Chem. Soc.*, 2011, **133**, 14998–15007.
11 K. Maeda, M. Eguchi, W. J. Youngblood and T. E. Mallouk, *Chem. Mater.*, 2009, **21**, 3611–3617.
12 Y. Okamoto, S. Ida, J. Hyodo, H. Hagiwara and T. Ishihara, *J. Am. Chem. Soc.*, 2011, **133**, 18034–18037.
13 J. Meurigá Thomas, *Chem. Commun.*, 2006, 3273–3278.
14 S. Liang, L. Wen, S. Lin, J. Bi, P. Feng, X. Fu and L. Wu, *Angew. Chem.*, 2014, **126**, 2995–2999.
15 T. Sasaki and M. Watanabe, *J. Am. Chem. Soc.*, 1998, **120**, 4682–4689.
16 F. Geng, R. Ma, Y. Yamauchi and T. Sasaki, *Chem. Commun.*, 2014, **50**, 9977–9980.
17 M. A. Bizeto, A. L. Shiguihara and V. R. Constantino, *J. Am. Chem. Soc.*, 2009, **19**, 2512–2525.
18 Z. Zhai, C. Hu, X. Yang, L. Zhang, C. Liu, Y. Fan and W. Hou, *J. Mater. Chem.*, 2012, **22**, 19122–19131.
19 T. Orzali, M. Casarin, G. Granozzi, M. Sambi and A. Vittadini, *Phys. Rev. Lett.*, 2006, **97**, 156101.
20 E. L. Tae, K. E. Lee, J. S. Jeong and K. B. Yoon, *J. Am. Chem. Soc.*, 2008, **130**, 6534–6543.
21 S. Liang, S. Zhu, Y. Chen, W. Wu, X. Wang and L. Wu, *J. Mater. Chem.*, 2012, **22**, 2670–2678.
22 K. Sakakibara, J. P. Hill and K. Ariga, *Small*, 2011, **7**, 1288–1308.
23 S. Acharya, J. P. Hill and K. Ariga, *Adv. Mater.*, 2009, **21**, 2959–2981.
24 T. Sasaki, M. Watanabe, H. Hashizume, H. Yamada and H. Nakazawa, *Chem. Commun.*, 1996, 229–230.
25 M. Leng, Y. Chen and J. Xue, *Nanoscale*, 2014, **6**, 8531–8534.
26 K. Nakagawa, T. Jia, W. Zheng, S. M. Fairclough, M. Katoh, S. Sugiyama and S. C. E. Tsang, *Chem. Commun.*, 2014, **50**, 13702–13705.
27 C. Hu, L. Zhang, L. Cheng, J. Chen, W. Hou and W. Ding, *J. Energy Chem.*, 2014, **23**, 136–144.
28 P. Liu, H. Zhang, H. Liu, Y. Wang, X. Yao, G. Zhu, S. Zhang and H. Zhao, *J. Am. Chem. Soc.*, 2011, **133**, 19032–19035.
29 R. E. Schaak and T. E. Mallouk, *Chem. Mater.*, 2000, **12**, 3427–3434.
30 G. B. Saupe, C. C. Waraksa, H.-N. Kim, Y. J. Han, D. M. Kaschak, D. M. Skinner and T. E. Mallouk, *Chem. Mater.*, 2000, **12**, 1556–1562.
31 P. Shen, H. Zhang, H. Liu, J. Xin, L. Fei, X. Luo, R. Ma and S. Zhang, *J. Mater. Chem. A*, 2015, **3**, 3456–3464.
32 K. Akatsuka, G. Takanashi, Y. Ebina, M.-a. Haga and T. Sasaki, *J. Phys. Chem. C*, 2012, **116**, 12426–12433.
33 F. Geng, R. Ma, A. Nakamura, K. Akatsuka, Y. Ebina, Y. Yamauchi, N. Miyamoto, Y. Tateyama and T. Sasaki, *Nat. Commun.*, 2013, **4**, 1632.
34 F. Geng, R. Ma, Y. Ebina, Y. Yamauchi, N. Miyamoto and T. Sasaki, *J. Am. Chem. Soc.*, 2014, **136**, 5491–5500.
35 H. Yuan, D. Dubbink, R. Besselink and J. E. ten Elshof, *Angew. Chem., Int. Ed.*, 2015, **54**, 9239–9243, DOI: 10.1002/anie.201502539.
36 E. M. Sabio, R. L. Chamousis, N. D. Browning and F. E. Osterloh, *J. Phys. Chem. C*, 2012, **116**, 3161–3170.
37 T. Oshima, D. Lu, O. Ishitani and K. Maeda, *Angew. Chem., Int. Ed.*, 2015, **54**, 2698–2702.

